THE JOURNAL OF PHYSICAL CHEMISTRY B

Article

pubs.acs.org/JPCB

Small Angle X-ray Scattering Investigation of Norbornene-Terminated Syndiotactic Polypropylene and Corresponding Comb-Like Poly(macromonomer)

Finizia Auriemma,* Claudio De Rosa, Rocco Di Girolamo, and Amelia Silvestre

Dipartimento di Scienze Chimiche, Università di Napoli "Federico II", Complesso Universitario Monte S. Angelo, via Cintia, I-80126 Napoli, Italy

Amelia M. Anderson-Wile and Geoffrey W. Coates

Department of Chemistry and Chemical Biology, Baker Laboratory, Cornell University, Ithaca, New York 14853-1301, United States

Supporting Information

ABSTRACT: The structure and crystallization properties of a norbornene end-functionalized syndiotactic polypropylene (sPP) macromonomer (MMsPP) with [*rrrr*] = 80 mol % and molecular mass M_n = 3600 g/mol and corresponding comb-like poly(macromonomer) (pMMsPP) with M_n = 100000 g/mol have been investigated using wide angle (WAXS) and small angle (SAXS) X-ray scattering, atomic force (AFM), transmission electron (TEM), and optical (OM) microscopy. The analysis reveals the tendency of the macromonomer and poly(macromonomer) to form structures characterized by layers of sPP chains alternated to layers occupied by the cyclic groups (norbornene or polynorbornene), and a small degree of interdigitation of sPP chains belonging to adjacent layers facing each other in an end-to-end arrangement. It is argued that this layering is dictated, upon crystallization, by nanophase separation of the flexible sPP chains in regions apart from those occupied by the cyclic groups coupled to formation of sPP crystals organized in the lamellar morphology. SAXS measurements indicate that in isothermally crystallized samples the layered structures are irregular and include sPP lamellar crystals of uniform thickness separated by amorphous layers whose thickness values have a multimodal distribution. These properties are intrinsic to the chemical structure of our systems and are only minimally influenced by the topological constrains of the covalent bonding of macromonomers in the corresponding comb-polymer.

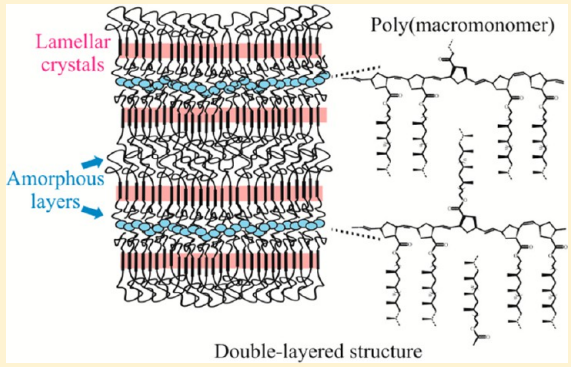

INTRODUCTION

Comb-polymers are macromolecules with a nonlinear chain architecture, comprising a main chain with multiple trifunctional branch points from each of which a linear side-chain emanates. For comb-polymers characterized by a backbone with dense and regularly spaced long side chains,[1−11] the backbone tends to assume highly extended conformations as a consequence of crowding of the long branches around the chain skeleton. The resulting global shape of highly branched macromolecules is often a compact cylinder or worm-like structure for chain backbones longer than the lateral diameter and a disk- or star-like shape for backbones of very short length.[1−14] In fact, the regular presence of long-chain branches per repeat unit of the polymer backbone induces large steric repulsions between adjacent side chains so that even highly flexible backbones acquire a high degree of rigidity, with values of the persistence length higher than the chain diameter.[12−32]

The solution and bulk properties of densely branched comb-polymers have been extensively studied.[15−39] The low values of intrinsic viscosity $[\eta]$ of their solutions with respect to linear polymers having identical composition and same molecular mass,[33,34] has been attributed to the fact that densely branched comb-polymers adopt more compact conformations than those of equivalent linear polymers, with shapes corresponding to spheres or cylinders at low and high molecular mass, respectively.[15−17,23−36] The lowering of glass transition temperature of amorphous branched chains with respect to the linear chains of similar molecular mass has been attributed to the increase of free volume because of the presence of an increased number of chain ends as a result of their branched architecture.[35,36] The peculiar linear dynamical response of densely branched comb-polymers with absence of entanglement plateau even for systems with total molecular mass larger than the critical molecular mass for entanglements has been

Received: May 3, 2013
Revised: June 25, 2013
Published: July 31, 2013

   dx.doi.org/10.1021/jp404394y | *J. Phys. Chem. B* 2013, 117, 10320−10333

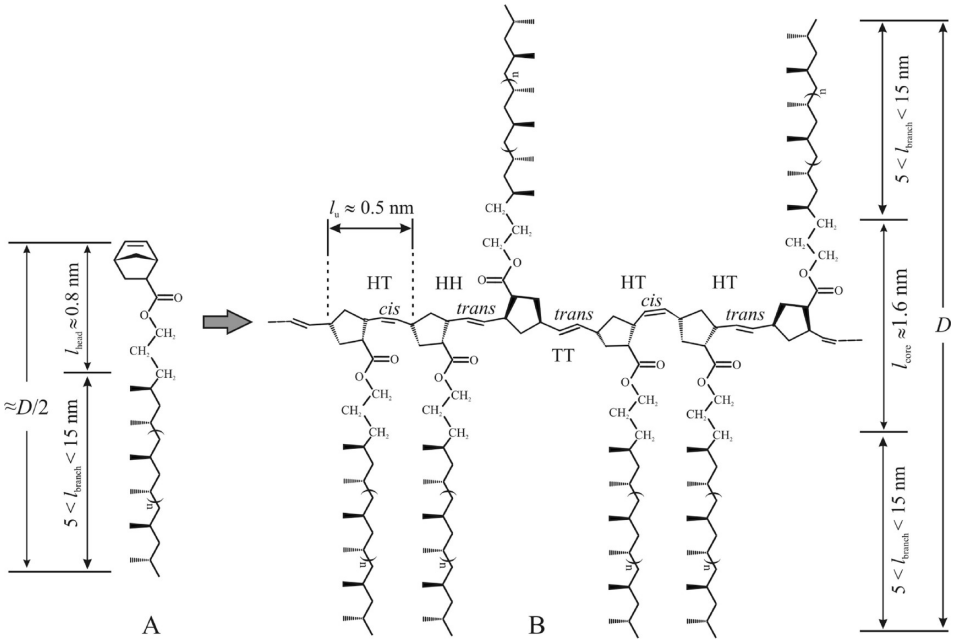

Figure 1. Chemical structure of the norbonene-terminated sPP macromonomer MMsPP (A) and corresponding poly(macromonomer) pMMsPP (B). The poly(macronomer) in B is characterized by head-to-tail HT, head-to-head HH and tail-to-tail TT enchainment, cyclopentylene rings in *cis* configuration (retained from the monomer), the vinylene moiety possessing *cis/trans* isomerism, and consecutive cyclopentylenes existing in either *meso* or *racemo* dyads. The average sizes of the cyclic terminals (l_{head}), sPP side chains (l_{branch}), core diameter (l_{core}), and average periodicity parallel to the chain axis (l_u) in the macromonomer (A) and corresponding poly(macromonomer) (B) are indicated (see Supporting Information). The lateral extension of the poly(macronomer) D (B) and the length of the macromonomer ≈ $D/2$ (A) are also indicated.

attributed to the fact that the linear rheological behavior of comb-systems is essentially controlled by the relaxation of the side chains.[15−17,36−39]

The solid state properties of comb-polymers with crystallizable side chains have also been studied,[40−63] especially in the case of comb-polymers containing *n*-alkyl groups as side chains.[47−63] It has been pointed out that, regardless of chemical nature and intrinsic flexibility of the backbone, comb-polymers with long *n*-alkyl side chains generally form layered structures made up of alternating crystalline and amorphous regions. The crystalline layers are formed by the side chains, whereas the amorphous layers contain the main chains aligned in a nearly planar arrangement and, on either side of these average planes, regions populated by the noncrystallizing portions of the side chains directly linked to the backbone.[47−63]

In this paper we focus on the study of the structural organization in the solid state of a comb-polymer consisting of crystallizable side chains of syndiotactic polypropylene (sPP) linked to a polynorbornene main chain via ester linkages (see Figure 1). This polymer has been prepared as described in ref 64 using the "grafting through" method[1−10,13,14,65,66] that involves the independent preparation of the side chains with a suitable functional end group, followed by their successive polymerization to a poly(macromonomer). More precisely, as shown in ref 64, allyl-terminated sPP macromonomers have been prepared using a nonliving bis(phenoxyimine)titanium catalyst activated by methylaluminoxane (MAO).[67,68] After conversion of end-functionalized polymers to hydroxyl- and, subsequently, norbornene-terminated macromonomers, syndiotactic polypropylene comb-polymers have been synthesized through ring-opening metathesis polymerization (ROMP) of the norbornene-functionalized polypropylene using a Grubbs catalyst.[12−14,65,66,69−78] To the best of our knowledge, this was the first report of a comb-polymer from end-functionalized syndiotactic polypropylene.[64]

The chemical structure of norbornene terminated sPP macronomer and of the corresponding poly(macronomer) is shown in Figure 1. A preliminary characterization of norbornene terminated sPP macromonomers and corresponding poly(macromonomers) has been already reported in ref 64. It has been shown that the poly(macromonomer) displays interesting thermal properties with both melting and crystallization temperatures lower and glass transition temperature higher than those of the corresponding macromonomer.[64] Furthermore, the crystallization rate of the poly(macromonomer) is 2−3 times lower than that of the corresponding macromonomer under isothermal conditions.[64] This behavior has been attributed to a decrease in mobility of the side chains in the comb polymer due to the constrains imposed by the rigid backbone, in agreement with the increase of glass transition temperature.[64]

In the present study, the characterization is extended to the analysis of the structure and morphology of these systems at different length scales using wide angle (WAXS) and small angle (SAXS) X-ray scattering, atomic force (AFM), transmission electron (TEM), and optical (OM) microscopy. In particular, the structural organization at nanometric length scale is investigated in detail in the case of a norbornene terminated sPP macromonomer and the corresponding poly(macromonomer) by performing SAXS analysis. The aim is to study the effect of the constraints imposed by the rigid comb-polymer backbone on the relative arrangement of sPP crystals and amorphous regions.

■ EXPERIMENTAL SECTION

The synthesis, solution ^{13}C NMR characterization, GPC analysis and DSC measurements of the analyzed norbornene-

dx.doi.org/10.1021/jp404394y | J. Phys. Chem. B 2013, 117, 10320−10333

terminated sPP macromonomer and poly(macromonomer) samples have been already described in detail in ref 64. The principal characteristics of the end-functionalized norbornene macromonomer (MMsPP) and of the corresponding poly(macromonomer) (pMMsPP) are reported in Table 1. They correspond to the samples exo-MM-3600−80 and PM-3600−80 of ref 64. The norbornene-terminated macromonomer contains norbornene rings bridged via an ester linkage to the sPP chains (see Figure 1A). It is characterized by moderate tacticity (fully syndiotactic pentads [*rrrr*] = 0.80) and average molecular mass M_n = 3600 g/mol. The corresponding poly(macromonomer) has number average molecular mass of 100000 g/mol. Although the exact configuration of the substituted poly(1,3-cyclopentylenevinylene) backbone of the poly(macromomer) obtained by ring-opening metathesis polymerization (ROMP) may not be established directly from solution NMR analysis due to the low concentration of norbornene residues, the chains of pMMsPP are regio- and stereoirregular.[79,80] As shown in Figure 1B, these chains are characterized by head-to-tail HT, head-to-head HH, and tail-to-tail TT enchainments, cyclopentylene rings in *cis* configuration (retained from the monomer), the vinylene moiety possessing *cis*/*trans* isomerism and consecutive cyclopentylenes existing in either *meso* or *racemo* dyads.[79,80]

Table 1. Norbornene Terminated Syndiotactic Polypropylene Macromonomer (MMsPP) and Corresponding Poly(macronomer) (pMMsPP) Characterization[64]

sample	M_n[a] (g/mol)	M_w/M_n[a]	[*rrrr*][b]	T_c[c] (°C)	T_m[c] (°C)
MMsPP	3600	1.87	0.80	65	112
pMMsPP	100000[d]	1.27	0.80	50	101

[a]Molecular weight (M_n) and molecular weight distribution (M_w/M_n) were determined by gel permeation chromatography at 140 °C in 1,2,4-trichlorobenzene relative to polyethylene standards. The polymerization reaction of pMMsPP was prolonged for 24 h. As shown in ref 64, even though the presence of small amount of unreacted macromonomer in the poly(macronomer) sample may not be excluded, for polymerization times longer than 2 h, the residual macromonomer was almost completely absent in the GPC chromatograph. [b]Syndiotacticity ([*rrrr*]) was determined using ^{13}C NMR spectroscopy. [c]Determined by DSC analysis at scanning rate of 10 °C/min. The melting temperature is relative to the second heating scan.[64] [d]The number average molecular mass of the sample pMMsPP corresponds to a lower limit due to the fact that eluate fractions with identical hydrodynamic volume correspond to molecular masses that for branched polymers are lower than those of linear polyethylene used for the calibration.

Melt pressed films with uniform thickness of ≈1 mm have been prepared by melting as prepared samples at 180 °C for 10 min under a press and cooling to room temperature by fluxing cold water within the hot plates. The pressure applied under the press has been regulated in such a way to avoid preferred orientation in the films, and at the same time to minimize formation of nanovoids and surface imperfections.

Isothermal crystallizations at different temperatures T_c have been conducted on compression molded films using a thermal bath. Under a N_2 atmosphere, compression molded films were melted at 200 °C, kept for 5 min at this temperature, and then rapidly cooled to the crystallization temperature T_c. The samples were kept at the crystallization temperature T_c for a time t_c (at least 24 h), well beyond the maximum time t_{max}, which was estimated in independent DSC experiments reported in ref 64, to allow complete crystallization at T_c. The samples were then rapidly cooled to room temperature for the successive analyses. Melt pressed films of some selected samples were also isothermally crystallized at different T_c directly in the high vacuum camera of the SAXS equipment using a nearly identical protocol (i.e., 5 min at 200 °C, rapid cooling, at −40 °C/min rate, to the crystallization temperature T_c, crystallization time t_{max}). We checked that SAXS data obtained for samples isothermally crystallized in situ were identical to those collected for the films crystallized ex situ in the same conditions.

X-ray powder diffraction profiles have been obtained with Ni filtered Cu Kα radiation using an automatic Philips diffractometer. Crystallinity (x_c(WAXS)) was determined from the powder diffraction profiles by the ratio between the crystalline diffraction area (A_c) and the area of the whole diffraction profiles (A_t), $x_c = (A_c/A_t) \times 100$. The area of the crystalline diffraction (A_c) has been determined by subtracting the area of the amorphous halo from the area of the whole diffraction profiles (A_t). The diffraction profiles of the amorphous phase were constructed by collecting X-ray powder diffraction profiles of melted samples in the temperature range 150−180 °C, and by successive extrapolation of these data to room temperature to account for the thermal expansion of amorphous/molten state.

SAXS measurements were performed on isothermally crystallized films cut in the shape of elongated sheets filling the whole sample holder. SAXS data of isothermally crystallized films were collected using an evacuated high performance SAXS instrument "SAXSess" (Anton Paar KG, Graz, Austria), which is a modification[81] of the so-called "Kratky compact camera".[82] Data collection has been performed in the slit collimation configuration with SAXSess camera attached to a conventional X-ray source (Cu Kα, wavelength λ = 1.5418 Å). The scattered radiation was recorded on a BAS-MS imaging plate (Fujifilm) in a configuration which allows recording simultaneous WAXS and SAXS data and is processed with a digital imaging reader (Perkin-Elmer Cyclone Plus Phosphor Imager) at a resolution in the small angle region of ≈60 nm (=$2\pi/q_{min}$, with q_{min} the minimum accessible value of scattering vector permitted by our collimation set up, equal to 0.1 nm^{-1} and $q = 4\pi \sin\theta/\lambda$, 2θ being the scattering angle). After subtraction for dark current, the empty sample holder, and a constant background due to thermal density fluctuations, the slit smeared data in the SAXS region (for $q < 4$ nm^{-1}) were deconvolved with the primary beam intensity distribution using the SAXSquant 2.0 software to obtain the corresponding pinhole scattering (desmeared) intensity distribution. SAXS measurements have been performed both at crystallization temperature T_c and at room temperature.

The wide angle regions recorded simultaneously with SAXS data have not been "desmeared", because the software used works in the infinite slit length approximation and, at high q, this approximation may not be used. However, we have checked that the position of Bragg reflections, the width at half-height of the peaks and the overall shape of diffraction profiles for $q > 7$ nm^{-1} are not greatly affected by use of the slit collimation configuration instead of the pinhole geometry. We have confirmed that the indices of crystallinity (x_c) determined from the X-ray powder diffraction profiles obtained with the line collimation geometry and the slit configurations are identical within the experimental error (3−5%).

Optical microphotographs of the samples have been recorded at room temperature in polarized light using a Zeiss Axioscop40 microscope equipped with a Mettler FP82 hot stage, by sandwiching a small amount of the samples in between a microscopy slide and a coverslip, after melting at ≈190 °C, rapid cooling to 100 °C and isothermal crystallization at this temperature for at least 2 h.

Polymer films (with a thickness of 50−100 nm) have been also prepared via drop casting from 0.2 and 0.5 wt % *p*-xylene solution on a glass slide. The surface morphology of as cast films and of these films after melting and crystallization to room temperature were analyzed using a Veeco Caliber AFM. The AFM analysis was also extended to films that were isothermally crystallized at different crystallization temperatures T_c. Images were recorded in tapping mode at room temperature with use of standard silicon cantilevers TESP-MT, tips with radius of ≈8 nm, at resonant frequency and force constant of about 250 kHz and 50 N m^{-1}, respectively.

"As cast" films have been analyzed by transmission electron microscopy (TEM) using a Philips EM 208S TEM with an accelerating voltage of 120 kV. To enhance contrast, the thin films were shadowed by Pt at an angle of 60°, coated with carbon, backed with a poly(acrylic acid), floated on water and mounted on a copper grid for TEM observations. As cast films have also been subjected to melting and recrystallization. TEM analyses were also performed on the melt-recrystallized thin films after decoration with gold nanoparticles by a vacuum deposition method. The deposition of gold particles on the surface of the copolymer film has been realized by thermal evaporation of gold and condensation under high vacuum (about 9×10^{-5} mbar). The films were positioned at a distance of 15 cm from a gold filament wrapped around a tungsten filament. A voltage value slightly above the minimum needed to bring tungsten filament to incandescence was applied for 2−3 s, to avoid melting of the polymer sample. Pt shadowing, carbon coating and gold decoration have been performed using an Emitech K950X thermal evaporator.

RESULTS AND DISCUSSION

Morphology. The crystallization ability of sPP chains in the macromonomer MMsPP as well as the poly(macronomer) pMMsPP have been probed at all length scales. In Figure 2, the typical POM images of MMsPP and pMMsPP samples are shown. The images were collected at room temperature for samples isothermally crystallized at T_c = 100 °C from the melt. In both cases, birefringent entities are observed, corresponding to spherulites formed at T_c covered by additional spherulites of lower diameter that develop during cooling to room temperature. In spite of the topological restrains, the spherulites formed by pMMsPP at the same crystallization temperature appear better developed than those formed by MMsPP. According to the results of ref 64, these differences may be due to the slower crystallization kinetics of the poly(macromonomer) than the macromonomer. The delayed crystallization of pMMsPP, indeed, produces a lower density of nuclei, which, in turn, gives rise to crystals growing even more slowly, thus producing larger and better spherulites than the macromonomer.

As shown by the corresponding X-ray powder diffraction profiles (Figure 2C), both samples are crystallized from the melt at T_c = 100 °C mainly in the normal antichiral form I of sPP[83−87] with a crystallinity index around 30%. X-ray diffraction profiles similar to those of Figure 2C have been obtained for

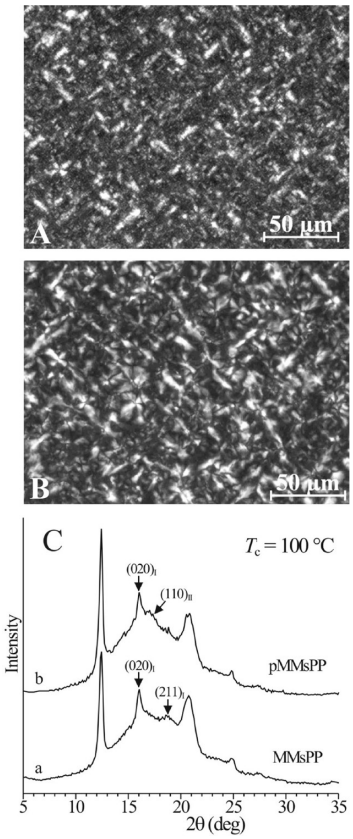

Figure 2. Optical microphotographs recorded at room temperature in polarized light (crossed polars) of the sPP macomonomer MMsPP (A) and poly(macromonomer) pMMsPP (B) for samples isothermally crystallized from the melt at 100 °C, and corresponding X-ray powder diffraction profiles (C). The $(020)_I$ and $(211)_I$ reflections of form I and $(110)_{II}$ reflection of form II of sPP are indicated in C.

samples isothermally crystallized at different T_c in ref 64. The crystallization of form I is indicated by the presence of the 200, 020, and 220 + 121 reflections at $2\theta \approx 12$, 16, and 21°, respectively.[84−87] For the macromonomer at T_c =100 °C (see ref 64 for a detailed discussion), more ordered crystalline modifications of form I of sPP in the alternation of right and left-handed helical chains along the axes of the unit cell are obtained, as indicated by the presence of the 211 reflection at 2θ = 18.8° in the diffraction profile a of Figure 2C.[87]

In the case of the poly(macromonomer), more disordered modifications of form I crystallize, as indicated by the absence of the 211 reflection at 2θ = 18.8° and small amounts of crystals of the isochiral form II[88,89] are formed, as indicated in the X-ray diffraction profile b of Figure 2C by the presence of the 110 reflection at 2θ = 17°, typical of the isochiral form II.[83,88,89] As argued in ref 64, the partial crystallization of form II in the sample pMMsPP is probably due to the reduced mobility of the backbone chain of the comb-shaped poly(macromonomer) whose side chains experience crystallization in a more constrained environment than the macromonomer, and the major ability of the isochiral form II to withstand compressive forces when compared with the antichiral form I.[90]

Thin films of the MMsPP and pMMsPP samples with thickness of 50−100 nm were obtained by drop casting 0.2 wt % *p*-xylene solutions on a glass substrate followed by slow evaporation of the solvent at room temperature. Low resolution Pt shadowed TEM images of the films are reported in Figure

dx.doi.org/10.1021/jp404394y | J. Phys. Chem. B 2013, 117, 10320−10333

3A,B. A cobweb superstructure made up of branched filaments with long and short branches is apparent.

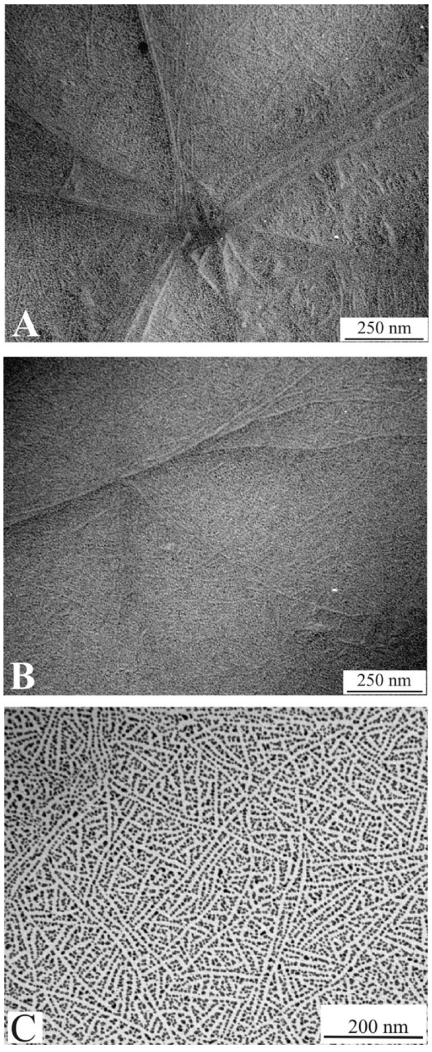

Figure 3. (A, B) Pt shadowed TEM images of thin films of MMsPP (A, A′) and pMMsPP (B, B′; 50−100 nm thick) obtained by drop casting 0.2 wt % *p*-xylene solutions on a glass substrate followed by slow evaporation of the solvent at room temperature. (C) TEM image of the solution cast thin film of the poly(macromonomer) after melting, recrystallization, and gold decoration on the surface.

The cobweb structure is confirmed by AFM phase images of these films, shown in Figure 4A,B. Nodular entities are also apparent in the AFM images of Figure 4. In the case of the macromonomer MMsPP, isolated filaments and nodules emerging from a uniform substrate are visible (left region of Figure 4A). These images are typical of our systems regardless of crystallization conditions. In fact, the AFM images obtained for films recrystallized from the melt are similar to those of Figure 4.

From the TEM and AFM images of Figures 3A,B and 4A,B, we distinguish thin filaments of width 20−30 nm, which assembled to form filaments 2−4 times wider extending in all directions. The length of filaments, instead, achieves values of the order of micrometers. Although the cross-sectional analysis of the corresponding AFM height images is affected by large errors due to our standard setup of AFM apparatus and the close distance of filaments in the case of poly-

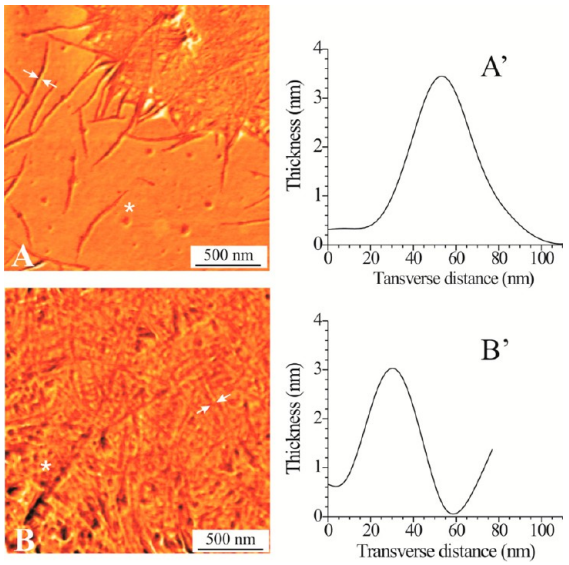

Figure 4. AFM phase images of thin films of MMsPP (A) and pMMsPP (B), 50−100 nm thick, obtained by drop casting 0.2 wt % (A) and 0.5 wt % (B) *p*-xylene solutions on a glass substrate followed by slow evaporation of the solvent at room temperature, and examples of cross-sectional analysis (A′,B′) of the filaments arrowed in A and B, respectively. In A and B, the asterisks indicate nodular entities.

(macromonomer),[91] it indicates that the typical heights of the filaments (averaged over ≈50 measurements) are, roughly, at least 3−4 nm (see, for instance, Figure 4A′,B′).

It is worth noting that the AFM images of Figure 4A,B are typical of bulk of sPP[91,92] and reflect the formation of lamellar crystals. However, in our case, the width of the filaments, around 20−30 nm, is of the same order of magnitude as the maximum value of the diameter D of pMMsPP cylinders (Figure 1B) and almost twice the maximum length of MMsPP macromonomers, in the limiting hypothesis that the sPP chains form extended chain crystals in a perfect **s**(2/1)2 helical conformation (lamellar thickness $l_{max} \approx 15$ nm, see Supporting Information). Therefore, considering that extended chain crystals are highly improbable due to the low degree of stereoregularity ([*rrrr*] = 80%) of sPP chains in our samples, the width of filaments, as visualized by TEM and AFM images of Figures 3 and 4, cannot correspond to the thickness of sPP lamellar crystals.

We argument that, similar to other comb-polymers with crystallizable side chains,[40−63] these filaments arise from self-assembly of MMsPP and pMMsPP chains in aggregates characterized by the alternation of layers of crystallizable sPP chains and amorphous layers where the polynorbornene backbone in the poly(macromonomer) and norbornene rings in the macromonomer are segregated, as shown in Figure 5. The layered structures formed upon crystallization in our systems are dictated by nanophase separation of the flexible sPP chains in regions apart from those occupied by the cyclic groups (norbornene units or cyclopentylene rings)[93] coupled to formation of sPP crystals organized in the lamellar morphology.

The layers may run either parallel to the filaments as in Figure 5A,B or normal to the filaments as in Figure 5A′,B′. The TEM images of Figure 3A,B and the AFM images of Figure 4 do not allow discriminating between the models of Figure 5. In fact, both models are able to explain the formation of long

dx.doi.org/10.1021/jp404394y | *J. Phys. Chem. B* 2013, 117, 10320−10333

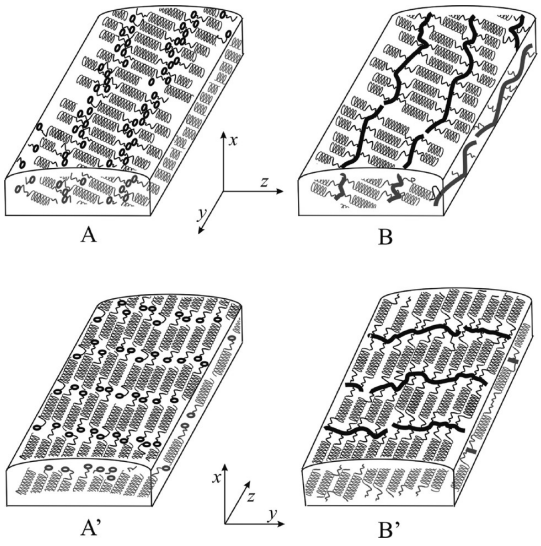

Figure 5. Limit models of the layered structure of the norbornene terminated macromonomer MMsPP (A, A′) and comb-like poly(macronomer) pMMsPP (B, B′) in the crystalline state. In all cases, the norbornene rings of macromonomers and the cyclopentylene rings of the poly(macronomer) are segregated in layers separated by layers containing the sPP chains, and form entities elongated along an axis (filaments). The direction normal to the layers is indicated with *z*. The layered structures are elongated, forming filaments in the direction *y* perpendicular to the layer normal (*z*) in the models A and B, and in the direction *z* parallel to the layer normal in the models A′ and B′. The sPP side chains are represented as helices.

filaments oriented in all directions and their organization in a cob-web superstructure stabilized by the formation of lamellar crystals of sPP. The main difference relies in that the layered structures are elongated forming filaments in the direction *y* perpendicular to the layer normal (*z*) in the models of Figure 5A,B, in the direction *z* parallel to the layer normal, in the models of Figure 5A′,B′. The widths of the filaments would correspond to the direction *z* parallel to the layer normal in the models of Figure 5A,B and to the direction *y* perpendicular to the layer normal in the models of Figure 5A′,B′.

It is worth noting that physical association of comb-polymers to form filamentous or cyclic dimeric or multimeric aggregates has already been described and directly viewed in the case of monolayered films of densely branched comb-systems of di- and triblock copolymers. Examples of filamentous or cyclic aggregates include the diblock copolymer poly(octadecyl methacrylate)-*b*-poly(2-(2-bromo-propionyloxy)ethyl methacrylate-*g*-poly(*n*-butylacrylate)), pODMA-*b*-(pBEP-*g*-nBUA), the triblock copolymer pODMA-*b*-(pBEP-g-nBUA)-*b*-pODMA,[94] and some graft polymers with poly(ε-caprolactone) (PCL) and PCL-*b*-poly(*n*-butyl acrylate) as side chains.[95] It was argued that such association is driven by the van der Waals attraction of the pODMA chain ends[94] and also due to crystallization of the relatively long octadecyl side chains in ref 94 and PCL side chains in ref 95. In particular, crystallization of PCL side chains with stems in the direction normal to the filamentous aggregates was inferred by direct AFM analysis.[95] This suggests that the models of Figure 5A,B are more plausible than the models of Figure 5A′,B′.

Formation of the sPP lamellar crystals is confirmed by the TEM images of thin films of pMMsPP obtained by solution casting and decorated with gold by standard vacuum evaporation and condensation on the polymer films. An example is shown in Figure 3C in the case of the sample pMMsPP, where the gold decoration reveals the morphology typical of semicrystalline polymers. Gold decoration is a technique normally used to enhance the surface topography of semicrystalline polymers and to improve the contrast between amorphous and crystalline phases, revealing the lamellar morphology.[96−98] As decoration patterns arise from reduced nucleation barrier at the edges and steps of crystals or in the areas of low interfacial energy,[97] in the TEM image of Figure 3C the crystalline lamellae appear as white stripes of thickness 5−7 nm oriented in all directions and separated by darker strips of the amorphous phase covered by Au nanoparticles. Similar images have been obtained in the case of the sample MMsPP.

SAXS and WAXS Analysis of Isothermally Melt-Crystallized Samples. The lamellar morphology of samples MMsPP and pMMsPP isothermally crystallized from the melt at different crystallization temperatures T_c has been analyzed by performing SAXS measurements. The SAXS data of the melt-crystallized samples were collected at the crystallization temperature T_c at the end of the crystallization and then at room temperature after cooling. The SAXS profiles of melt-crystallized samples of MMsPP and pMMsPP, multiplied by the Lorentz factor after background subtraction and desmearing (see Experimental Section), are reported in Figure 6.

WAXS profiles of samples MMsPP and pMMsPP were recorded simultaneously to the SAXS data at the crystallization temperature T_c and are also shown in Figure 6C. The WAXS data are similar to those recorded at room temperature on the same melt-crystallized samples and reported in ref 64. Moreover, apart from the different geometry used for collection, they contain the same information shown in Figure 2C. As already discussed above, indeed, the macromonomer MMsPP crystallizes from the melt in form I of sPP at any crystallization temperature and tends to crystallize in more ordered modifications of form I with increasing the crystallization temperature T_c (Figure 6C). Samples of the poly(macromonomer) pMMsPP also crystallize mainly in form I but a small amounts of crystals of the isochiral form II[88,89] are also obtained (Figure 6C′).

The values of crystallinity index of each melt-crystallized sample, evaluated from the WAXS profiles, at the crystallization temperature T_c and at room temperature, are reported in Table 2. We observe that upon cooling from the crystallization temperature T_c to room temperature, the values of crystallinity index x_c of the isothermally melt-crystallized samples increase by ≈17−30% regardless of the value of T_c. The crystallinity index is, indeed, ≈21−22% for both samples at T_c and is ≈30% in the case of the macromonomer and ≈26% in the case of the poly(macromonomer) at room temperature. This increase of crystallinity is not due to incomplete crystallization of the samples at a given T_c but it is rather due to secondary crystallization (vide infra).[99]

The Lorentz-corrected SAXS intensity distribution of the isothermally crystallized samples at various T_c of Figure 6 show in all cases a correlation peak typical of a periodically layered morphology in agreement with the layered structure inferred by morphological analysis. The SAXS profiles of the samples collected at the crystallization temperature T_c are sharp and have well-defined shapes (Figure 6B,B′), whereas the SAXS intensity collected at room temperatures are broad and show rather composite shapes, presenting shoulders especially in the

dx.doi.org/10.1021/jp404394y | J. Phys. Chem. B 2013, 117, 10320−10333

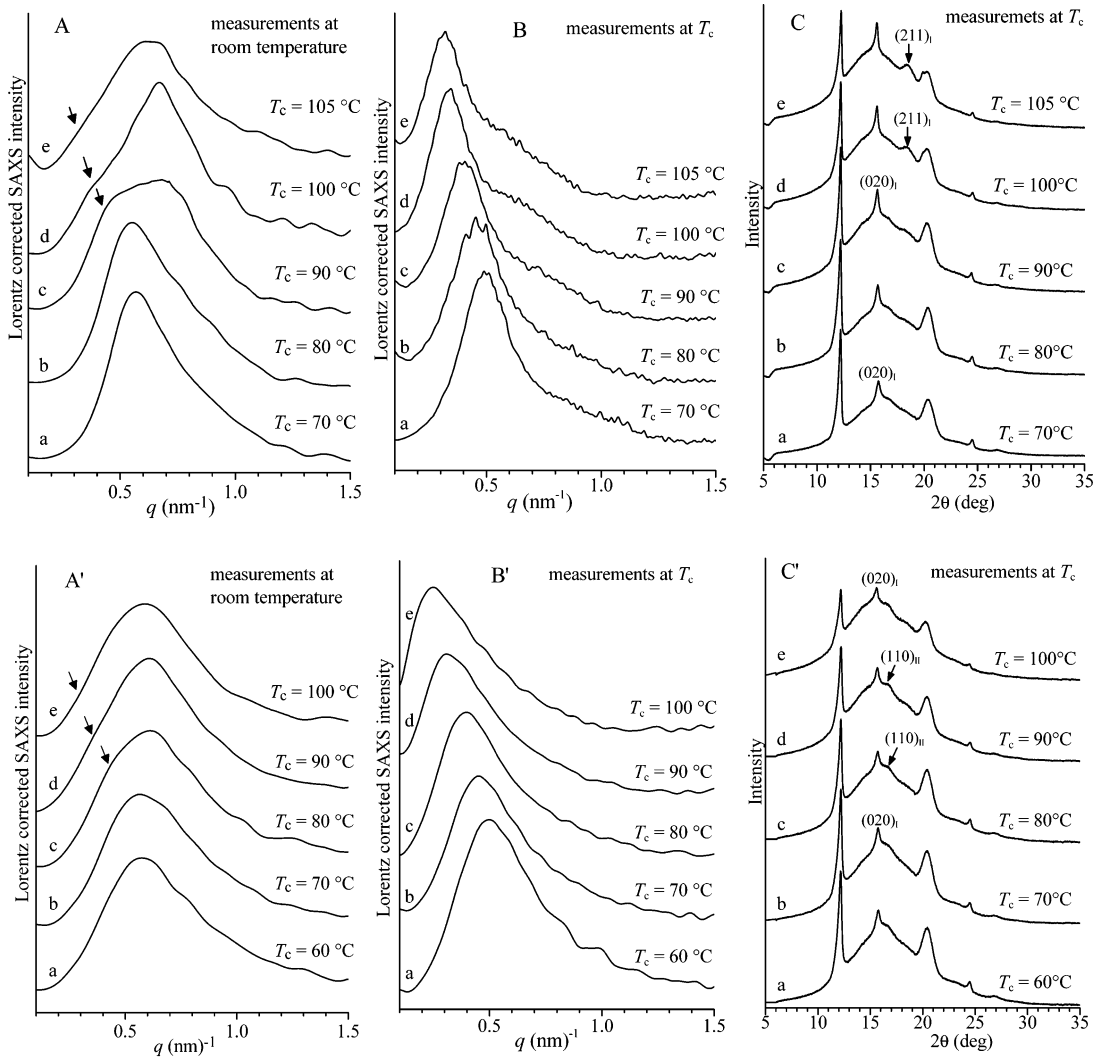

Figure 6. Lorentz-corrected SAXS profiles (A, B, A′, B′) and corresponding WAXS profiles (C, C′) of samples of the macromonomer MMsPP (A–C) and of the corresponding poly(macromonomer) pMMsPP (A′–C′) isothermally crystallized from the melt at the indicated crystallization temperatures (T_c), recorded at the crystallization temperature T_c at the end of the crystallization (B, B′) and at room temperature after cooling (A, A′). Only the WAXS profiles recorded at the crystallization temperature T_c are shown in C and C′. The $(020)_I$ and $(211)_I$ reflections of form I and $(110)_{II}$ reflection of form II of sPP are indicated in C and C′. Arrows in A and A′ indicate shoulders in the low q range relative to the correlation peak of the crystals formed at T_c.

low q region (curves c, d of Figure 6A and curve c of Figure 6A′).

The position of the maxima q^* of the SAXS peaks are reported in Table 2. It is apparent that the position of the maxima q^* of the SAXS correlation peak measured at T_c gradually shifts to low values of q with increasing T_c (Figure 6B,B′). This shift is only partially related to the thermal expansion of the random coil chains in the amorphous regions,[100,101] but it is also due to the normal increase of crystal thickness with the crystallization temperature and possible rearrangements of the layered structures. For SAXS data measured at room temperature, the value of q^* does not greatly depend on T_c and establishing its exact value is less obvious due to the intrinsic broadness of the maxima (Figure 6A,A′).

In the hypothesis that the unidimensional layered structure of our samples can be interpreted in terms of a two-phase lamellar model, consisting of laterally extended sPP crystallites of thickness t_c alternating to amorphous layers of thickness t_a (see Figure S3), the average lamellar periodicity $P = t_c + t_a$ has been evaluated resorting to three methods, that is, from the position of maxima q^*, using the Bragg law, as $P = 2\pi/q^*$, by calculation of the one-dimensional normalized (self-) correlation function of electron density fluctuations $\gamma(z)$,[102] and the distribution function of distances between interfaces IDF.[103] In this modeling, the amorphous layers, that include the cyclic groups (norbornene or polynorbornene) with the pendant $-COO-(CH_2)_3$-linkages and the noncrystallizing sPP portions of chains (see Figure S3) have been assumed of uniform electron density along the direction normal to the layers.

The correlation function $\gamma(z)$ extracted from SAXS data measured at T_c of isothermally crystallized samples are reported in Figure 7A,B. The values of the periodicity P and lamellar thickness t_c achieved by our samples in isothermal crystallization at various T_c, obtained from the position of the secondary maximum and the main correlation triangle of the correlation function $\gamma(z)$ (Figure 7A,B; see Supporting Information) are reported in Figure 8A as a function of T_c

dx.doi.org/10.1021/jp404394y | J. Phys. Chem. B 2013, 117, 10320–10333

Table 2. Crystallinity Index (x_c) and Volume Fraction of Crystalline Phase (φ_c), Peak Position (q^*) in the SAXS Profiles of Figure 6, Average Periodicity of the Layered Structure (P), Specific Inner Surface (S/V), Lamellar Thickness (t_c), and Thickness of Amorphous Layers (t_a) of Samples of Macromonomer MMsPP and Corresponding Poly(macromonomer) pMMsPP Isothermally Crystallized from the Melt at the Temperatures T_c

	room temperature measurements					measurements at T_c												
	experimental data									correlation function				interface distribution function				
T_c (°C)	x_c (%)	φ_c [a]	q^* (nm^{-1})	P (nm)	S/V (nm^{-1})	x_c (%)	φ_c [a]	q^* (nm^{-1})	P (nm)	P (nm)	t_c (nm)	t_a (nm)	φ_c [b]	P [c] (nm)	t_c (nm)	t_a (nm)	φ_c [b]	S/V (nm^{-1})
Macromonomer																		
70	28	0.26	0.56	11	0.20	22	0.21	0.49	12.8	12.3	3.5	8.8	0.28	11.8	3.6	≈8	0.29	0.17
80	28	0.26	0.55	11	0.22	22	0.21	0.46	13.7	13.5	3.8	9.7	0.28	12.5	3.9		0.31	0.15
90	30	0.28	0.60	10	0.23	19	0.18	0.40	15.7	15.2	4.1	11.1	0.27	14.0	4.3	≈11	0.31	0.13
100	30	0.28	0.66	10	0.29	20	0.19	0.33	19.0	18.2	4.3	13.9	0.24	16.2	4.3	≈12	0.27	0.12
105	29	0.27	0.63	10	0.35	19	0.18	0.31	20.3	19.5	4.5	15.0	0.23	16.9; 22.4	4.5	≈13	0.26	0.11
Polymacromonomer																		
60	26	0.24	0.58	11	0.25	22	0.21	0.50	12.6	12.3	3.0	9.3	0.24	9.05; 12.2	2.78	≈6		0.17
70	24	0.22	0.58	11	0.24	19	0.18	0.45	14.0	13.2	3.3	9.9	0.25	11.9; 15.9	2.98	≈7		0.16
80	24	0.22	0.60	10	0.25	21	0.20	0.40	15.7	15.2	3.6	11.6	0.24	10.6; 13.4 17.4	3.6	≈8		0.14
90	25	0.23	0.60	10	0.23	21	0.20	0.33	19.0	19.2	4.1	15.1	0.21	13.7; 17.8	3.7	≈10		0.11
100	26	0.24	0.57	11	0.24	18	0.17	0.25	25.1	29.9	4.5	25.4	0.15	15; 21; 26.	3.8	≈12		0.07

[a]Evaluated as $\varphi_c = (x_c/d_c)/[(x_c/d_c) + (1 - x_c)/d_a]$, with d_c and d_a, as the density of the crystalline[18] and amorphous phases, equal to 0.93 and 0.85 g/cm^3, respectively. The values of density have been assumed constant with temperature. [b]Evaluated as the ratio of lamellar thickness t_c and the average periodicity of the layered structures P. [c]The IDF shows multiple minima that have been attributed to the multimodal distribution of thickness of amorphous layers.

(curves a–c) and Table 2. It is apparent that the values of P calculated from the correlation function $\gamma(z)$ are nearly identical to the values of P evaluated from the position q^* of maxima in the Lorentz corrected SAXS intensity distribution of Figure 6B,B′ (squared symbols of Figure 8A and Table 2).

As shown in Figure 8A and Table 2, the values of lamellar thickness of the macromonomer and the corresponding poly(macromonomer) (curve a of Figure 8A) gradually increase with the crystallization temperature from 3.0 to 4.5 nm and, at any T_c, are nearly identical. On the contrary, at any given T_c, the values of the average periodicity P for the poly(macromonomer) (curve c of Figure 8A) are always higher than those achieved by the macromonomer (curve b of Figure 8A) and these differences increase with increasing T_c.

More precisely, the values of P are in all cases higher than 12 nm and increase with increase of the crystallization temperature up to values of $P \approx 20$ nm for the macromonomer (curve b of Figure 8A) and $P \approx 25–30$ nm for the poly(macromonomer) (curve c of Figure 8A). It is worth noting that, in the limiting hypothesis of fully crystallizable sPP moieties, the utmost extension of the macromonomer and poly(macromonomer) in the direction normal to the layers would be ≈16 nm ($=(l_{branch})_{max} + l_{core}/2$, see Figure 1 and Supporting Information). Because crystallization of fully extended chain crystals of sPP is unreliable, due in part to the relatively low degree of stereoregularity of our samples, values of average periodicity as high as 25–30 nm achieved for the samples isothermally crystallized from the melt at high temperatures suggest that the MMsPP and pMMsPP chains tend to arrange forming double layered structures with a scarce degree of interpenetration of sPP chains belonging to adjacent layers, and only at the lowest T_c, sPP chains belonging to adjacent layers are, at least in part, interpenetrated.

The higher values in the layer periodicity P of poly(macromonomer) in respect to macromonomer at any T_c probably reflect a different degree of interpenetration of the sPP chains belonging to adjacent layers, and the fact that, in the case of the poly(macromonomer), in order to alleviate mutual repulsions of adjacent branches, deviations from the unperturbed dimensions of the sPP side chains in the amorphous regions close to the backbone toward stretched conformations are expected. Moreover, differences in P values may also originate from the major difficulties experienced by sPP branches in the poly(macromonomer) in the crystallization process due to the topological constraints of the chain backbone, resulting in the formation of layered structures less compact and regular than those obtained in the case of the macromonomer at the same crystallization conditions.

Deviations of the layer structure of our samples from a regular one is clearly indicated by the distribution function of distances (IDF) between interfaces extracted from SAXS data of Figure 6B,B′ (Figure 7C,D). The IDF functions of Figure 7C,D indeed show positive and negative peaks versus the interface distance.[103–105] The first two positive peaks correspond to the distribution functions of the thickness of the crystalline and amorphous layers (centered at t_c and t_a). However, whereas in the case of the macromonomer samples isothermally crystallized at low temperatures (curves a–d of Figure 7C) the positive peaks are followed by a negative peak corresponding to the distribution function of the periodicity $P = t_c + t_a$, as expected for regular layer structures (see Supporting Information), in the case of the poly(macromonomer) pMMsPP (Figure 7D) and for the macromonomer MMsPP

dx.doi.org/10.1021/jp404394y | J. Phys. Chem. B 2013, 117, 10320–10333

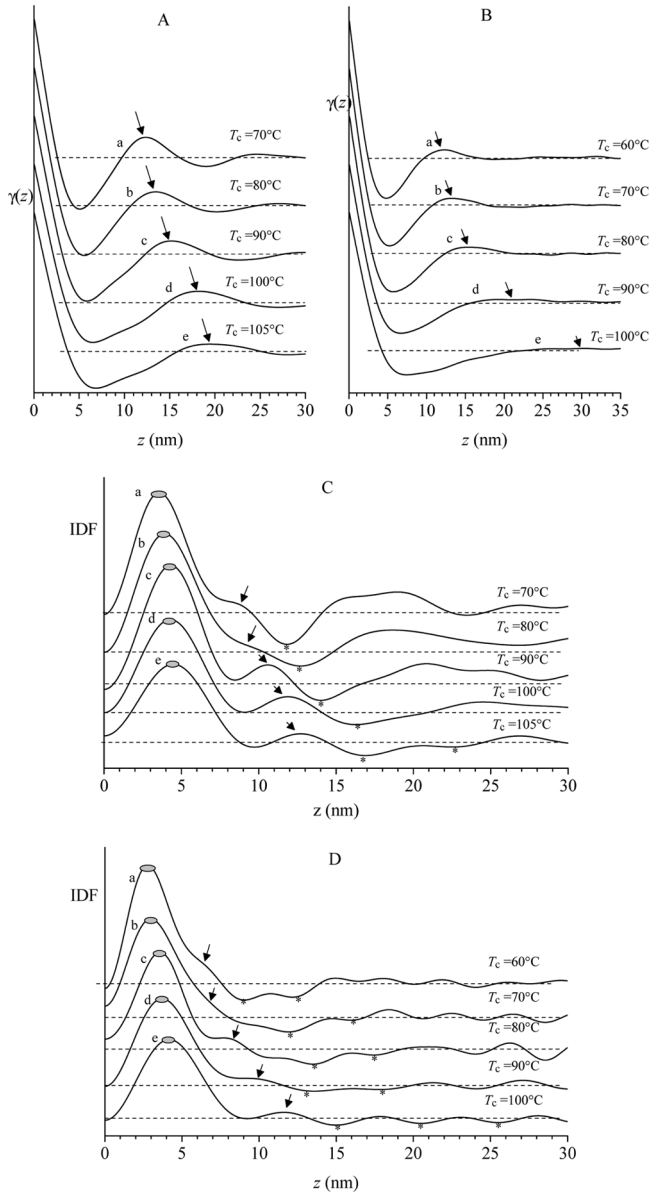

Figure 7. Normalized correlation functions of electron density $\gamma(z)$ (A, B) and distribution function of interface distances (IDF; C, D) as a function of interlayer correlation distance (z), extracted from SAXS data measured at T_c in the case of samples of the macromonomer MMsPP (A, C) and the corresponding poly(macromonomer) pMMsPP (B, D) isothermally crystallized from the melt at the indicated values of crystallization temperatures T_c. The average periodicity P of the layered structures are indicated with an arrow in A, B, whereas the dashed lines define the zero of $\gamma(z)$ and IDF functions in A–D.

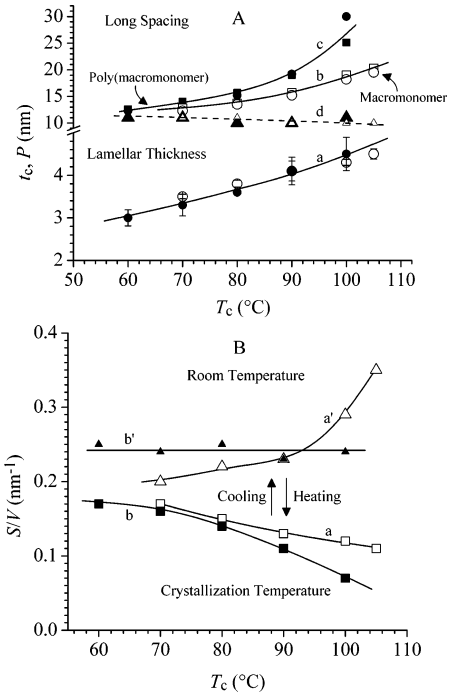

Figure 8. (A) Values of the average periodicity (P) and lamellar thickness (t_c) of the layered structures formed by isothermal crystallization from the melt at different crystallization temperatures (T_c) in samples of the macromonomer MMsPP (○,□,Δ) and of the corresponding poly(macromonomer) pMMsPP (●,■,▲) measured at T_c at the end of the crystallization (a–c) and at room temperature after cooling (d), as a function of the crystallization temperature. The values of the average periodicity evaluated from the position q^* of maxima in the Lorentz corrected SAXS curves, using the Bragg law ($P = 2\pi/q^*$) (□,■,Δ,▲) and the average periodicity P and the lamellar thickness t_c extracted from the one-dimensional normalized correlation function of electron density fluctuations $\gamma(z)$ (○,●) are indicated. (B) Specific inner surface (S/V) of the layered structures formed by isothermal crystallization from the melt at different crystallization temperature (T_c) in samples of the macromonomer MMsPP (□,Δ) and of the corresponding poly(macromonomer) pMMsPP (■,▲) measured at T_c at the end of the crystallization process (a,b) and at room temperature after cooling (a′,b′) as a function of the crystallization temperature.

crystallized at high temperatures (curve e of Figure 7C) instead of having a single negative peak at P, we have a multiplicity of negative peaks (indicated with an asterisk), suggesting that the layer structure that develops by isothermal conditions in our systems is not regular. This irregular structure may be modeled as made up of sPP lamellar crystals of uniform thickness t_c separated by amorphous layers having a broad distribution function of thickness that instead of being centered around a single value t_a, as in a regular layer structure, is centered around a multiplicity of values t_{a1}, t_{a2}, t_{a3}, and so on.

A general model to explain the multimodal distribution of the thicknesses of amorphous layers is shown in Figure 9A. In this model, the electron density profile $\rho(z)$ probed by a line traveling across the interfaces in the direction perpendicular to the layers (z) is non periodic (Figure 9A′). This vertical line, indeed, probes crystalline regions of electron density ρ_c with a narrow thickness distribution centered at t_c alternating to amorphous layers of electron density ρ_a and variable thickness whose distribution function show multiple peaks centered at t_{a1}, t_{a2}, t_{a3}, and so on. From the IDF profiles of Figure 7C,D, it is not easy distinguishing the various contributions from these complex layered structures, since the distribution functions of the thickness of amorphous layers are broad, and are buried by the negative contributions due to distribution of interface distances occurring every pair of consecutive phases, centered at $t_c + t_{a1}$, $t_c + t_{a2}$, $t_c + t_{a3}$, and so on. Also, these latter distributions are expected to be broad. Therefore, in Figure 8C,D, only the most frequent interface distances are discernible.[103,104]

dx.doi.org/10.1021/jp404394y | J. Phys. Chem. B 2013, 117, 10320–10333

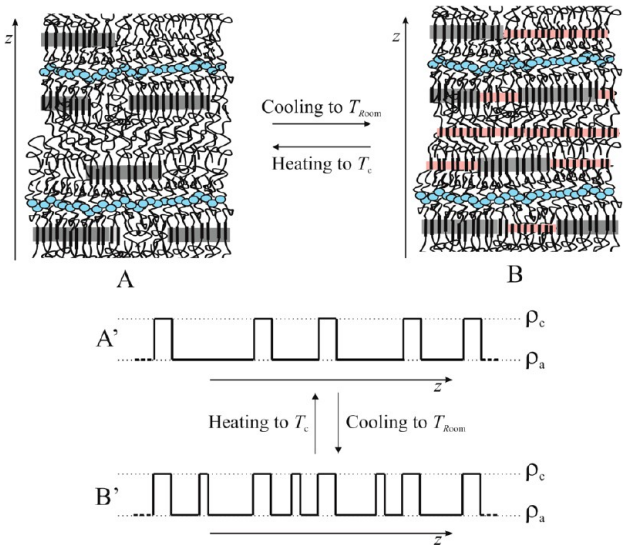

Figure 9. Models of the layer structures that develop in the macromonomer MMsPP and poly(macromonomer) pMMsPP by isothermal crystallization at high temperatures (A) and corresponding evolution achieved upon cooling at room temperature (B). (A′, B′) Electron density profiles probed by a line crossing the models A and B, respectively, in a direction (z) normal to the layers, with ρ_c and ρ_a the electron density of crystalline and amorphous regions, respectively.

Upon cooling to room temperature, the isothermally crystallized samples (Figure 6B,B′), the apparent values of the average periodicity P of the layered structure of both MMsPP and pMMsPP samples decrease to around 10 nm, regardless of crystallization temperature used for their preparation (curve d of Figure 8A and Table 2). Furthermore, the values of P determined at room temperature are scarcely dependent on the crystallization temperature and, with increasing T_c, they decrease rather than increase. The change of the average periodicity of the layered structure is reversible in consecutive cycles made up of a cooling step from T_c to room temperature followed by the heating step to T_c and is due to formation of new crystals at room temperature, that melt in the successive heating step up to T_c. The crystals formed by this secondary crystallization may either form inside the amorphous regions included into the layer structure formed at any given T_c and the extra layer amorphous regions.[99,105]

To shed light on the mechanism subtending this secondary crystallization, we have calculated the value of the specific inner surface[105] S/V of our samples from SAXS data measured at T_c at the end of the crystallization process and at room temperature (see Supporting Information). They are reported in Table 2 and Figure 8B. It is apparent that the values of specific inner surface of the macromonomer and the corresponding poly(macromonomer) determined at the end of crystallization process decrease with increase of crystallization temperature (curves a,b of Figure 8B) in agreement with the increase of the average periodicity of the layer structure P with T_c (curves b, c of Figure 8A). Indeed, at any T_c, the values of specific inner surface are nearly coincident with two times the inverse of periodicity P ($S/V \approx 2/P$), as expected for a two-phase lamellar structure characterized by sharp interfaces (see Table 2).[103,105] Upon cooling to room temperature, the values of specific inner surface increase and this increase is higher the higher is the crystallization temperature (curves a′,b′ of Figure 8B) and deviate from the ideal value $2/P$ by a factor k ($=PS/2V$), which is nearly constant ($k \approx 1.3$) in the case of the poly(macromonomer), and comprised in the range 1.1−1.8 in the case of the macromonomer. The increase of specific inner surface and decrease of periodicity P upon cooling to room temperature after isothermal crystallization is the hallmark that the new lamellar crystals are mainly formed inside the amorphous regions included inside the layer structure formed at any given T_c. A model showing secondary crystallization through the insertion mechanism inferred by the present analysis is shown in the model of Figure 9B. The new crystals formed in the interlamellar amorphous regions are thinner than the preexisting ones formed at T_c and therefore undergo reversible melting upon cooling the sample to T_c.

CONCLUSIONS

The structural organization in the solid state of a norbornene-terminated syndiotactic polypropylene macromonomer and of the corresponding comb-like poly(macromonomer) synthesized by ROMP using a Grubbs catalyst has been investigated at different length scales. The crystallization of sPP chains takes place within layered structures guided by the tendency of the cyclic groups (norbornene units in the macromonomer, cyclopentylene groups in the poly(macromonomer)) to associate forming filamentous micellar aggregates of contour length much longer than the backbone length of the comb-polymer in the maximum extension and width of the same order of its transversal dimensions. The sPP chains belonging to adjacent layers exhibit a scarce degree of interpenetration.

Surface analysis of 50−100 nm thin films obtained by drop casting of dilute solutions of the macromonomer and poly(macromonomer) followed by successive melting/recrystallization reveals that these filaments form a cob-web network. In a filament, long sPP side chains participate as lamellar crystals or coiled amorphous regions of the same filament and coexist with sPP side chains which participate as crystals and/or amorphous regions of adjacent non parallel filaments, thus, creating the physical junctions of the network. Whether this network structure is created by some kind of microphase separation already occurring in the melt due to the low compatibility of flexible sPP chains and the cyclic groups[93] or driven by crystallization of sPP is difficult to distinguish from our experiments. However, because both processes are feasible and become highly probable with decreasing the temperature, we argue that they happen almost simultaneously and act synergistically to fix the final morphology.

SAXS analysis reveals that the distribution function of lamellar thicknesses of sPP crystals formed by isothermal crystallization is centered around a single value, whereas the distribution function of lamellar thicknesses of amorphous layers is multimodal. These irregular structures arise from the intrinsic tendency of norbonene rings in the macromonomer, cyclopentylene rings in the polymacronomer to segregate in layers that are well separated from the layers occupied by the sPP chains, so that at any crystallization temperatures, formation of more regular and compact lamellar structures are prevented, and also complete rejection of the most irregular sPP sequences from intralamellar amorphous regions is hindered. In other terms, whereas in a normal crystallization process the most irregular portion of chains may be easily rejected into the interlamellar amorphous phase, the intrinsic layering tendency of macromonomer and poly-

dx.doi.org/10.1021/jp404394y | J. Phys. Chem. B 2013, 117, 10320−10333

(macromonomer) makes this rejection mechanism more difficult, especially in the case of the comb-polymer.

The present investigation is the first detailed study on the effect of bulky, poorly compatible terminal groups in a stereoregular olefin macromonomer on the crystallization properties and morphology of sPP. At the same time, it is also the first report on the morphology and crystallization properties of a comb-polymer in which sPP branches emanate with a high frequency (1 branch/5 carbon atoms) from a backbone consisting of units poorly compatible with the side chains. Because the sPP chains have average molecular mass of less than 4000 g/mol, crystallization of sPP takes place from a poorly entangled melt.[106] Therefore, we have studied crystallization of sPP from a disentangled melt. Formation of extended crystals in our samples was unfortunately prevented by the relatively low stereoregularity of the chains and the polydispersity of molecular mass.

We have shown that the preparation of end-functionalized stereoregular macromonomers and successive polymerization of these macromonomers to poly(macromonomers) represents a useful tool toward basic studies aimed at understanding the role of nanophase separation versus crystallization of stereoregular polyolefins from disentangled melts, both prior to and after polymerization to comb-like polymers. Besides, potential applications of comb-polymers carrying stereoregular vinyl polymers as side chains such as isotactic polypropylene or polybutene may be envisaged in their use as additive to facilitate processing of important commercial polymers, blend compatibilizer, stabilizers of dispersions, and so on to obtain at low cost materials with improved performance (see, for instance, refs 107−111).

■ ASSOCIATED CONTENT

Supporting Information

Geometrical Considerations; Analysis of SAXS data; Evaluation of correlation function of electron density; Evaluation of the distribution function of distances between interfaces (IDF). This material is available free of charge via the Internet at http://pubs.acs.org.

■ AUTHOR INFORMATION

Corresponding Author

*Tel.: ++39 081 674341. Fax ++39 081 674090. E-mail: finizia.auriemma@unina.

Notes

The authors declare no competing financial interest.

■ ACKNOWLEDGMENTS

G.W.C. gratefully acknowledges support from National Science Foundation (DMR-0706578). F.A. and C.D.R. gratefully acknowledge support from the "Ministero dell' Istruzione, dell'Università e della Ricerca" (PRIN2010). TEM measurements were carried out at C.I.S.M.E (Centro Interdipartimentale di Servizio per la Microscopia Elettronica) of the University of Napoli "Federico II".

■ REFERENCES

(1) Hadjichristidis, N.; Pitsikalis, M.; Pispas, S.; Iatrou, H. Polymers with Complex architecture by Living Anionic Polymerization. *Chem. Rev.* **2001**, *101*, 3747−3792.

(2) Sheiko, S. S.; Möller, M. Visualization of Macromolecules—A First Step to Manipulation and Controlled Response. *Chem. Rev.* **2001**, *101*, 4099−4123.

(3) Zhang, M.; Müller, A. H. E. Cylindrical Polymer Brushes. *J. Polym. Sci., Part A: Polym. Chem.* **2005**, *43*, 3461−3481.

(4) Voit, B. I.; Lederer, A. Hyperbranched and Highly Branched Polymer Architectures—Synthetic Strategies and Major Characterization Aspects. *Chem. Rev.* **2009**, *109*, 5924−5973.

(5) Peleshanko, S.; Tsukruk, V. V. The Architectures and Surface Behavior of Highly Branched Molecules. *Prog. Polym. Sci.* **2008**, *33*, 523−580.

(6) Sheiko, S. S.; Sumerlin, B. S.; Matyjaszewski, K. Cylindrical Molecular Brushes: Synthesis, Characterization, and Properties. *Prog. Polym. Sci.* **2008**, *33*, 759−785.

(7) Hadjichristidis, N.; Pitsikalis, M.; Iatrou, H.; Pispas, S. The Strength of the Macromonomer Strategy for Complex Macromolecular Architecture: Molecular Characterization, Properties, and Applications of Polymacromonomers. *Macromol. Rapid Commun.* **2003**, *24*, 979−1013.

(8) Huang, K.; Rzayev, J. Well-Defined Organic Nanotubes from Multicomponent Bottlebrush Copolymers. *J. Am. Chem. Soc.* **2009**, *131*, 6880−6885.

(9) Sarkar, D.; El Khoury, J. M.; Lopina, S. T.; Hu, J. Grafting Poly(*t*-butyl acrylate) to Poly(allylamine) by Iinverse Microemulsion Radical Polymerization: From Comb-Polymer to Amphiphilic Shell Cross-linked Polymer Nanocapsule. *J. Appl. Polym. Sci.* **2007**, *104*, 1905−1911.

(10) Yuan, J.; Lu, Y.; Schacher, F.; Lunkenbein, T.; Weiss, S.; Schmalz, H.; Müller, A. H. E. Template-Directed Synthesis of Hybrid Titania Nanowires within Core−Shell Bishydrophilic Cylindrical Polymer Brushes. *Chem. Mater.* **2009**, *21*, 4146−4154.

(11) Rzajev, J. Molecular Bottlebrushes: New Opportunities in Nanomaterials Fabrication. *ACS Macro Lett.* **2012**, *1*, 1146−1149.

(12) Runge, M. B.; Dutta, S.; Bowden, N. B. Synthesis of Comb Block Copolymers by ROMP, ATRP, and ROP and Their Assembly in the Solid State. *Macromolecules* **2006**, *39*, 498−508.

(13) Xia, Y.; Olsen, B. D.; Kornfield, J. A.; Grubbs, R. H. Efficient Synthesis of Narrowly Dispersed Brush Copolymers and Study of Their Assemblies: The Importance of Side Chain Arrangement. *J. Am. Chem. Soc.* **2009**, *131*, 18525−18532.

(14) Xia, Y.; Kornfield, J. A.; Grubbs, R. H. Efficient Synthesis of Narrowly Dispersed Brush Polymers via Living Ring-Opening Metathesis Polymerization of Macromonomers. *Macromolecules* **2009**, *42*, 3761−3766.

(15) Wintermantel, M.; Gerle, M.; Fischer, K.; Schmidt, M.; Wataoka, I.; Urakawa, H.; Kajiwara, K.; Tsukahara, Y. Molecular Bottlebrushes. *Macromolecules* **1996**, *29*, 978−983.

(16) Wintermantel, M.; Schmidt, M.; Tsukahara, Y.; Kajiwara, K.; Kohjiya, S. Rodlike Combs. *Macromol. Rapid Commun.* **1994**, *15*, 279−284.

(17) Tsukahara, Y.; Inoue, J.; Ohta, Y.; Kohjiya, S.; Okamoto, Y. Preparation and Characterization of α-Benzyl-ω-vinylbenzyl Polystyrene Macromonomer. *Polym. J.* **1994**, *26*, 1013−1018.

(18) Subbotin, A.; Saariabo, M.; Ikkala, O.; ten Brinke, G. Elasticity of Comb Copolymer Cylindrical Brushes. *Macromolecules* **2000**, *33*, 3447−3452.

(19) Saariaho, M.; Subbotin, A.; Szleizer, I.; Ikkala, O.; ten Brinke, G. Effect of Side Chain Rigidity on the Elasticity of Comb Copolymer Cylindrical Brushes: A Monte Carlo Simulation Study. *Macromolecules* **1999**, *32*, 4439−4443.

(20) Saariaho, M.; Subbotin, A.; Ikkala, O.; ten Brinke, G. Comb Copolymer Cylindrical Brushes Containing Semiflexible Side Chains. A Monte Carlo Study. *Macromol. Rapid Commun.* **2000**, *21*, 110−115.

(21) Saariaho, M.; Szleizer, I.; Ikkala, O.; ten Brinke, G. Extended Conformations of Isolated Molecular Bottle-Brushes. Influence of Side-Chain Topology. *Macromol. Theory Simul.* **1998**, *7*, 211−216.

(22) Saariaho, M.; Ikkala, O.; ten Brinke, G. Molecular Bottle Brushes in Thin Films: An Off-Lattice Monte Carlo Study. *J. Chem. Phys.* **1999**, *110*, 1180−1187.

(23) Denesyuk, N. A. Bottle-Brush Polymers as an Intermediate Between Star and Cylindrical Polymers. *Phys. Rev. E* **2003**, *68*, 031803/1−10.

(24) Denesyuk, N. A. Conformational Properties of Bottle-Brush Polymers. *Phys. Rev. E* **2003**, *67*, 051803/1−10.
(25) Rouault, Y.; Borisov, O. V. Comb-Branched Polymers: Monte Carlo Simulation and Scaling. *Macromolecules* **1996**, *29*, 2605−2611.
(26) Shiokawa, K.; Itoh, K.; Nemoto, N. Simulations of the Shape of a Regularly Branched Polymer as a Model of a Polymacromonomer. *J. Chem. Phys.* **1999**, *111*, 8165−8173.
(27) Khalatur, P. G.; Shirvanyanz, D. G.; Starovoitova, N. Yu.; Khokhlov, A. R. Conformational Properties and Dynamics of Molecular Bottle-Brushes: A Cellular-Automation-Based Simulation. *Macromol. Theory Simul.* **2000**, *9*, 141−155.
(28) Sheng, Y.-J.; Cheng, K.-L.; Ho, C.-C. Effect of Solvent Quality on the Conformations of a Model Comb Polymer. *J. Chem. Phys.* **2004**, *121*, 1962−1968.
(29) Lipson, J. E. G. A Monte Carlo Simulation Study on Long-Chain Combs. *Macromolecules* **1991**, *24*, 1327−1333.
(30) Lipson, J. E. G. Statistical and Metric Properties of Long-Chain Combs. *Macromolecules* **1993**, *26*, 203−207.
(31) Connolly, R.; Bellesia, G.; Timoshenko, E. G.; Kuznetosov, Y. A.; Elli, S.; Ganazzoli, F. Intrinsic and Topological Stiffness in Branched Polymers. *Macromolecules* **2005**, *38*, 5288−5299.
(32) Panyukov, S.; Zhulina, E. B.; Sheiko, S. S.; Randall, G. C.; Brock, J.; Rubinstein, M. Tension Amplification in Molecular Brushes in Solutions and on Substrates. *J. Phys. Chem. B* **2009**, *113*, 3750−3768.
(33) (a) Tsukahara, Y.; Kohijiya, K.; Tsutsumi, K.; Okamoto, Y. On the Intrinsic Viscosity of Poly(macromonomer)s. *Macromolecules* **1994**, *27*, 1662−1664.
(34) Lesne, T.; Heroguez, V.; Gnanou, Y.; Duplessix, R. Viscosimetric Study of Polystyrene Polymacromonomer Dilute Solutions. *Colloid Polym. Sci.* **2001**, *279*, 190−195.
(35) Tsukahara, Y.; Tsutsumi, K.; Okamoto, Y. On Some Bulk Properties of Poly(macromonomers). *Makromol. Chem., Rapid Commun.* **1992**, *13*, 409−413.
(36) Vlassopoulos, D.; Fytas, G.; Loppinet, B.; Issel, F.; Lutz, P.; Benoit, H. Polymacromonomers: Structure and Dynamics in Non-dilute Solutions, Melts, and Mixtures. *Macromolecules* **2000**, *33*, 5960−5969.
(37) Hu, M.; Xia, Y.; McKenna, G. B.; Kornfield, J. A.; Grubbs, R. H. Linear Rheological Response of a Series of Densely Branched Brush Polymers. *Macromolecules* **2011**, *44*, 6935−6943.
(38) Tsukahara, Y.; Namba, S.-i.; Iwasa, J.; Nakano, Y.; Kaeriyama, K.; Takahashi, M. Bulk Properties of Poly(macromonomer)s of Increased Backbone and Branch Lengths. *Macromolecules* **2001**, *34*, 2624−2629.
(39) Terao, K.; Farmer, B. S.; Nakamura, Y.; Iatrou, H.; Hong, K.; Mays, J. W. Radius of Gyration of Polystyrene Combs and Centipedes in a ϑ Solvent. *Macromolecules* **2005**, *38*, 1447−1450.
(40) Feng, L.-B; Zhou, S.-X.; You, B.; Wu, L.-M. Synthesis and Surface Properties of Polystyrene-*graft*-poly(ethylene glycol) Copolymers. *J. Appl. Polym. Sci.* **2007**, *103*, 1458−1465.
(41) Inomata, K.; Nakanishi, E.; Sakane, Y.; Koike, M.; Nose, T. Side-Chain Crystallization Behavior of Graft Copolymers Consisting of Amorphous Main Chain and Crystalline Side Chains: Poly(methyl methacrylate)-*graft*-poly(ethylene glycol) and Poly(methyl acrylate)-*graft*-poly(ethylene glycol). *J. Polym. Sci., Part B: Polym. Phys.* **2005**, *43*, 79−86.
(42) Reimschuessel, H. K. Glass Transition Temperature of Comblike Polymers: Effects of Side Chain Length and Backbone Chain Structure. *J. Polym. Sci., Part A: Polym. Chem.* **1979**, *17*, 2447−2457.
(43) Yan, Q.; Yuan, J.; Zhang, F.; Sui, X.; Xie, X.; Yin, Y.; Wang, S.; Wei, Y. Cellulose-Based Dual Graft Molecular Brushes as Potential Drug Nanocarriers: Stimulus-Responsive Micelles, Self-Assembled Phase Transition Behavior, and Tunable Crystalline Morphologies. *Biomacromolecules* **2009**, *10*, 2033−2042.
(44) Berthier, D. L.; Herrmann, A.; Ouali, L. Synthesis of Hydroxypropyl Cellulose Derivatives Modified with Amphiphilic Diblock Copolymer Side Chains for the Slow Release of Volatile Molecules. *Polym. Chem.* **2011**, *2*, 2093−2101.
(45) Kusumi, R.; Teramoto, Y.; Nishio, Y. Crystallization Behavior of Poly(ε-caprolactone) Grafted onto Cellulose Alkyl Esters: Effects of Copolymer Composition and Intercomponent Miscibility. *Macromol. Chem. Phys.* **2008**, *209*, 2135−2146.
(46) Bo, G.; Wesslen, B.; Wesslen, K. B. Amphiphilic Comb-Shaped Polymers from Poly(ethylene glycol) Macromonomers. *J. Polym. Sci., Part A: Polym. Chem.* **1992**, *30*, 1799−1808.
(47) Shi, H.; Zhao, Y.; Dong, X.; Zhou, Y.; Wang, D. Frustrated Crystallisation and Hierarchical Self-Assembly Behaviour of Comb-Like Polymers. *Chem. Soc. Rev.* **2013**, *42*, 2075−2099.
(48) Inomata, K.; Sakamaki, Y.; Nose, T.; Sasaki, S. Solid-State Structure of Comb-Like Polymers Having *n*-Octadecyl Side Chains. II. Crystalline-Amorphous Layered Structure. *Polym. J.* **1996**, *28*, 993−999.
(49) Hsieh, H. W. S.; Post, B.; Morawetz, H. A Crystallographic Study of Polymers Exhibiting Side-Chain Crystallization. *J. Polym. Sci., Polym. Phys. Ed.* **1976**, *14*, 1241−1255.
(50) Platè, N. A.; Shibaev, V. P. Comb-Like Polymers. Structure and Properties. *Macromol. Rev.* **1974**, *8*, 117−253.
(51) Zhou, Y.; Shi, H.; Men, Y.; Jiang, S.; Rotstegge, J.; Wang, D. Confined Crystallization and Phase Transition in Semi-Rigid Chitosan Containing Long Chain Alkyl Groups. *CrystEngComm* **2011**, *13*, 561.
(52) Stern, R.; Ballauff, M.; Lieser, G.; Wegner, G. Rigid-Rod Polymers with Flexible Side Chains. Synthesis, Structure and Phase Behavior of Poly(3-*n*-alkyl-4-oxybenzoates. *Polymer* **1991**, *32*, 2096−2115.
(53) März, K.; Lindner, P.; Urban, G.; Ballauff, M.; Kugler, J.; Fisher, E. W. Conformation and Shape of Rigid-Rod Polyesters Substituted with Flexible Side Chains as Revealed by Small-Angle Neutron Scattering. *Acta Polym.* **1993**, *44*, 139−147.
(54) Ballauff, M.; Schmidt, G. F. Rigid Rod Polymers Having Flexible Side Chains. 3. Structural Investigations on a Novel Layered Mesophase Formed by Thermotropic Poly(1,4-phenylene-2,5-dialkoxyterephthalate)s. *Mol. Cryst. Liq. Cryst.* **1987**, *147*, 163−177.
(55) Fujimori, A.; Chiba, S.; Sato, N.; Abe, Y.; Shibasaki, Y. Surface Morphological Changes in Monolayers of Aromatic Polyamides Containing Various *n*-Alkyl Side Chains. *J. Phys. Chem. B* **2010**, *114*, 1822−1835.
(56) Jordan, E. F., Jr.; Feldeisen, D. W.; Wrigley, A. N. Side-Chain Crystallinity. I. Heats of Fusion and Melting Transitions on Selected Homopolymers Having Long Side Chains. *J. Polym. Sci., Part A: Polym. Chem.* **1971**, *9*, 1835−1852.
(57) Jordan, E. F., Jr.; Artymyshyn, B.; Speca, A.; Wrigley, A. N. Side-Chain Crystallinity. II. Heats of Fusion and Melting Transitions on Selected Copolymers Incorporating *n*-Octadecyl Acrylate or Vinyl Stearate. *J. Polym. Sci., Part A: Polym. Chem.* **1971**, *9*, 3349−3365.
(58) Jordan, E. F., Jr. Side-Chain Crystallinity. III. Influence of Side-Chain Crystallinity on the Glass Transition Temperatures of Selected Copolymers Incorporating *n*-Octadecyl Acrylate or Vinyl Stearate. *J. Polym. Sci., Part A: Polym. Chem.* **1971**, *9*, 3367−3378.
(59) Jordan, E. F., Jr.; Riser, G. R.; Artymyshyn, B.; Pensabene, J. W.; Wrigley, A. N. Side-Chain Crystallinity. IV. Mechanical Properties and Transition Temperatures of Copolymers of Methyl Methacrylate with Higher *n*-Alkyl acrylates and N-*n*-Alkylacrylamides. *J. Polym. Sci., Part A: Polym. Chem.* **1972**, *10*, 1657−1679.
(60) Hempel, E.; Budde, H.; Horing, S.; Beiner, M. On the Crystallization Behavior of Frustrated Alkyl Groups in Poly(*n*-octadecyl methacrylate). *J. Non-Cryst. Solids* **2006**, *352*, 5013−5020.
(61) Hempel, E.; Budde, H.; Höring, S.; Beiner, M. Side Chain Crystallization in Microphase-Separated Poly(styrene-*block*-octadecyl methacrylate) Copolymers. *Thermochim. Acta* **2005**, *432*, 254−261.
(62) Mierzwa, M.; Floudas, G.; Stepanek, P.; Wegner, G. Effect of Pressure on the Side-Chain Crystallization of Poly(*n*-octadecyl methacrylate) Studied by Dielectric Spectroscopy. *Phys. Rev. B* **2000**, *62*, 14012−14019.
(63) Ruderer, M. A.; Prams, S. M.; Rawolle, M.; Zhong, Q.; Perlich, J.; Roth, S. V. Peter Müller-Buschbaum, P. Influence of Annealing and Blending of Photoactive Polymers on Their Crystalline Structure. *J. Phys. Chem. B* **2010**, *114*, 15451−15458.

(64) Anderson-Wile, A. M.; Coates, G. W.; Auriemma, F.; De Rosa, C.; Silvestre, A. Synthesis and Ring-Opening Metathesis Polymerization of Norbornene-Terminated Syndiotactic Polypropylene. *Macromolecules* **2012**, *45*, 7863−7877.
(65) (a) Jha, S.; Dutta, S.; Bowden, N. B. Synthesis of Ultralarge Molecular Weight Bottlebrush Polymers Using Grubbs' Catalysts. *Macromolecules* **2004**, *37*, 4365−4374.
(66) Cheng, X.; Ma, J.; Zhi, J.; Yang, X.; Hu, A. Synthesis of Novel "Rod−Coil" Brush Polymers with Conjugated Backbones through Bergman Cyclization. *Macromolecules* **2010**, *43*, 909−913.
(67) Cherian, A. E.; Lobkovsky, E. B.; Coates, G. W. Synthesis of Allyl-Terminated Syndiotactic Polypropylene: Macromonomers for the Synthesis of Branched Polyolefins. *Macromolecules* **2005**, *38*, 6259−6268.
(68) Hustad, P. D.; Tian, J.; Coates, G. W. Mechanism of Propylene Insertion Using Bis(phenoxyimine)-Based Titanium Catalysts: An Unusual Secondary Insertion of Propylene in a Group IV Catalyst System. *J. Am. Chem. Soc.* **2002**, *124*, 3614−3621.
(69) (a) Yoo, J.; Bowden, N. B. Synthesis of Comb Tri- and Tetrablock Copolymers Catalyzed by the Grubbs First Generation Catalyst. *Macromol. Rapid Commun.* **2009**, *30*, 1392−1398.
(70) Runge, M. B.; Lipscomb, C. E.; Ditzler, L. R.; Mahanthappa, M. K.; Tivanski, A. V.; Bowden, N. B. Investigation of the Assembly of Comb Block Copolymers in the Solid State. *Macromolecules* **2008**, *41*, 7687−7694.
(71) Yoo, J.; Runge, B.; Bowden, N. B. Synthesis of Complex Architectures of Comb Block Copolymers. *Polymer* **2011**, *52*, 2499−2504.
(72) Matson, J. B.; Grubbs, R. H. Synthesis of Fluorine-18 Functionalized Nanoparticles for use as in Vivo Molecular Imaging Agents. *J. Am. Chem. Soc.* **2008**, *130*, 6731.
(73) Johnson, J. A.; Lu, Y. Y.; Burts, A. O.; Xia, Y.; Durrell, A. C.; Tirrell, D. A.; Grubbs, R. H. Drug-Loaded, Bivalent-Bottle-Brush Polymers by Graft-through ROMP. *Macromolecules* **2010**, *43*, 10326−10335.
(74) Johnson, J. A.; Lu, Y. Y.; Burts, A. O.; Lim, Y.-H.; Finn, M. G.; Koberstein, J. T.; Turro, N. J.; Tirrell, D. A.; Grubbs, R. H. Core-Clickable PEG-Branch-Azide Bivalent-Bottle-Brush Polymers by ROMP: Grafting-Through and Clicking-To. *J. Am. Chem. Soc.* **2011**, *133*, 559−566.
(75) Montembault, D. L.; Soutif, J.-C.; Rutnakornpituk, M.; Fontaine, L. Synthesis of Well-Defined ω-Oxanorbornenyl Poly(ethylene oxide) Macromonomers via Click Chemistry and Their Ring-Opening Metathesis Polymerization. *Macromolecules* **2010**, *43*, 5611−5617.
(76) Li, Z.; Zhang, K.; Ma, J.; Cheng, C.; Wooley, K. L. Facile Syntheses of Cylindrical Molecular Brushes by a Sequential RAFT and ROMP "Grafting-Through" Methodology. *J. Polym. Sci., Part A: Polym. Chem.* **2009**, *47*, 5557−5563.
(77) Li, Z.; Ma, J.; Cheng, C.; Zhang, K.; Wooley, K. L. Synthesis of Hetero-Grafted Amphiphilic Diblock Molecular Brushes and their Self-Assembly in Aqueous Medium. *Macromolecules* **2010**, *43*, 1182−1184.
(78) Li, Z.; Ma, J.; Lee, N. S.; Wooley, K. L. Dynamic Cylindrical Assembly of Triblock Copolymers by a Hierarchical Process of Covalent and Supramolecular Interactions. *J. Am. Chem. Soc.* **2011**, *133*, 1228−1231.
(79) Amir-Ebrahimi, V.; Corry, D. A.; Hamilton, J. G.; Thompson, J. M.; Rooney, J. J. Characteristics of $RuCl_2(CHPh)(PCy_3)_2$ as a Catalyst for Ring-Opening Metathesis Polymerization. *Macromolecules* **2000**, *33*, 717−724.
(80) Delaude, L.; Demonceau, A.; Noels, A. F. Probing the Stereoselectivity of the Ruthenium-Catalyzed Ring-Opening Metathesis Polymerization of Norbornene and Norbornadiene Diesters. *Macromolecules* **2003**, *36*, 1446−1456.
(81) Bergmann, A.; Orthaber, D.; Scherf, G.; Glatter, O. Improvement of SAXS Measurements on Kratky Slit Systems by Gobel Mirrors and Imaging-Plate Detectors. *J. Appl. Crystallogr.* **2000**, *33*, 869−875.
(82) Kratky, O.; Stabinger, O. X-ray Small Angle Camera with Block-Collimation System, an Instrument of Colloid Research. *Colloid Polym. Sci.* **1984**, *262*, 345−360.
(83) De Rosa, C.; Auriemma, F. Structure and Physical Properties of Syndiotactic Polypropylene: A Highly Crystalline Thermoplastic Elastomer. *Prog. Polym. Sci.* **2006**, *31*, 145−237.
(84) Lotz, B.; Lovinger, A. J.; Cais, R. E. Crystal Structure and Morphology of Syndiotactic Polypropylene Single Crystals. *Macromolecules* **1988**, *21*, 2375−2382.
(85) De Rosa, C.; Corradini, P. Crystal Structure of Syndiotactic Polypropylene. *Macromolecules* **1993**, *26*, 5711−5718.
(86) Lovinger, A. J.; Lotz, B.; Davis, D. D.; Padden, F. J. Structure and Defects in Fully Syndiotactic Polypropylene. *Macromolecules* **1993**, *26*, 3494−3503.
(87) De Rosa, C.; Auriemma, F.; Vinti, V. Disordered Polymorphic Modifications of Form I of Syndiotactic Polypropylene. *Macromolecules* **1997**, *30*, 4137−4146.
(88) Corradini, P.; Natta, G.; Ganis, P.; Temussi, P. A. Crystal Structure of Syndiotactic Polypropylene. *J. Polym. Sci., Part C: Polym. Lett.* **1967**, *16*, 2477−2484.
(89) De Rosa, C.; Auriemma, F.; Vinti, V. On the Form II of Syndiotactic Polypropylene. *Macromolecules* **1998**, *31*, 7430−7435.
(90) Rastogi, S.; La Camera, D.; van der Burgt, F.; Terry, A. E.; Cheng, S. Z. D. Polymorphism in Syndiotactic Polypropylene: Thermodynamic Stable Regions for Form I and Form II in Pressure−Temperature Phase Diagram. *Macromolecules* **2001**, *34*, 7730−7736.
(91) (a) Ivanov, D. A.; Magonov, S. N. Atomic Force Microscopy Studies of Semicrystalline Polymers at Variable Temperature. *Lect. Notes Phys.* **2003**, *606*, 98−130.
(92) Marquardt, J.; Thomann, R.; Thomann, Y.; Heinemann, J. Mülhaupt Miscibility of Branched Ethene Homopolymers with Iso- and Syndiotactic Polypropenes. *Macromolecules* **2001**, *34*, 8669−8674.
(93) Shiniozaki, A.; Jasnow, D.; Balasz, A. Microphase Separation in Comb Copolymers. *Macromolecules* **1994**, *27*, 2496−2502.
(94) Qin, S.; Matyjaszewski, K.; Xu, H.; Sheiko, S. S. Synthesis and Visualization of Densely Grafted Molecular Brushes with Crystallizable Poly(octadecyl methacrylate) Block Segments. *Macromolecules* **2003**, *36*, 605−612.
(95) Yu-Su, S. Y.; Sheiko, S. S.; Lee, H.-i.; Jakubowski, W.; Nese, A.; Matyjaszewski, K.; Anokhin, D.; Ivanov, D. A. Crystallization of Molecular Brushes with Block Copolymer Side Chains. *Macromolecules* **2009**, *42*, 9008−9017.
(96) (a) Wittmann, J. C.; Lotz, B. Polymer Decoration: the Orientation of Polymer Folds as Revealed by the Crystallization of Polymer Vapors. *J. Polym. Sci., Polym. Phys. Ed.* **1985**, *23*, 205−226.
(97) Basset, G. A. A New Technique for Decoration of Cleavage and Slip Steps on Ionic Crystal Surfaces. *Philos. Mag.* **1958**, *3*, 1042−1045.
(98) Petermann, J.; Broza, G. Epitaxial Deposition of Metals on Uniaxial Oriented Semi-Crystalline Polymers. *J. Mater. Sci.* **1987**, *22*, 1108−1112.
(99) Fakirov, S.; Apostolov, A. A.; Boeske, P.; Zachmann, H. G. Structure of Segmented Poly(ether esters) as Revealed by Synchrotron Radiation. *J. Macromol. Sci., Part B: Phys.* **1990**, *29*, 379−395.
(100) Lovinger, A. J.; Lotz, B.; Davis, D. D.; Shumacher, M. Morphology and Thermal Properties of Fully Syndiotactic Polypropylene. *Macromolecules* **1994**, *27*, 6603−6611.
(101) Lacks, D. J.; Rutledge, G. C. Molecular Basis for the Anisotropic Transverse Thermal Expansion of Syndiotactic Polypropylene. *Macromolecules* **1995**, *28*, 5789−5792.
(102) Roe, R.-J. *Methods of X-ray and Neutron Scattering in Polymer Science*; Oxford University Press: New York, 2000.
(103) Ruland, W. The Evaluation of the Small-Angle Scattering of Lamellar Two-Phase Systems by Means of Interface Distribution Functions. *Colloid Polym. Sci.* **1977**, *255*, 417−427.
(104) Stribeck, N. *X-Ray Scattering of Soft Matter*; Springer-Verlag: Berlin, Heidelberg, 2007.
(105) Strobl, G. *The Physics of Polymers*; Springer: Berlin, 1996.

(106) From measurements of the plateau modulus, the molecular mass between consecutive entanglement M_e in sPP is ≈2200 g/mol, see, for instance Eckstein, A.; Suhm, J.; Friedrich, C.; Maier, R.-D.; Sassmannshausen, J.; Bochmann, M.; Mülahaupt, R. Determination of Plateau Moduli and Entanglement Molecular Weights of Isotactic, Syndiotactic, and Atactic Polypropylenes Synthesized with Metallocene Catalysts. *Macromolecules* **1998**, *31*, 1335−1340. However, recent results in collaboration with Nino Grizzuti (Department of Chemical Engineering, University of Naples Federico II) have pointed out that the value of M_e in sPP increases with [*rrrr*] and is around 4500 g/mol for sPP samples with [*rrrr*] = 80% (Amhad, R.; Di Girolamo R.; Auriemma, F.; De Rosa, C.; Grizzuti, N., manuscript in preparation).

(107) Lagendijk, R. P.; Hogt, A. H.; Buijtenhuijs, A.; Gotsis, A. D. Peroxydicarbonate Modification of Polypropylene and Extensional Flow Properties. *Polymer* **2001**, *42*, 10035−10043.

(108) Gahleitner, M. Melt Rheology of Polyolefins. *Prog. Polym. Sci.* **2001**, *26*, 895−944.

(109) Li, S.; Lynch, I.; Piculell, L. Effect of Hydrophilically Modified Graft Polystyrene on AOT Oil-Continuous Microemulsions: Viscosifying Effects of P(S-g-PEO) as a Function of Graft Chain Length and Graft Density. *J. Phys. Chem. B* **2004**, *108*, 15944−15951.

(110) Xiao, M.; Guan, Y.; Wei, D.; Xiao, H.; Zheng, A. A Novel Strategy for the Preparation of Long Chain Branching Polypropylene and the Investigation on Foamability and Rheology. *Eur. Polym. J.* **2012**, *48*, 362−371.

(111) Lyatskaya, Y.; Gersappe, D.; Gross, N. A.; Balazs, A. C. Designing Compatibilizers To Reduce Interfacial Tension in Polymer Blends. *J. Phys. Chem.* **1996**, *100*, 1449−1458.